Available online at www.sciencedirect.com
ScienceDirect
Journal of the European Ceramic Society 32 (2012) 9–26
www.elsevier.com/locate/jeurceramsoc

# Assembly of 8YSZ nanoparticles into gas-tight 1–2 μm thick 8YSZ electrolyte layers using wet coating methods

Tim Van Gestel *, Doris Sebold, Hans Peter Buchkremer, Detlev Stöver

*Forschungszentrum Jülich, Institute of Energy and Climate Research, IEK-1: Materials Synthesis and Processing, Leo-Brandt-Strasse, D-52425 Jülich, Germany*

Received 12 October 2010; received in revised form 18 June 2011; accepted 10 July 2011

**Abstract**

The application of a thin film electrolyte layer with a thickness in the micrometer range could greatly improve current solid oxide fuel cells (SOFCs) in terms of operating temperature and power output. Since the achievable minimal layer thickness with conventional powder coating methods is limited to ∼5 μm, a variety of thin film methods have been studied, but results on regular large-scale anode substrates are still lacking in the literature. In this paper, a wet coating process is presented for fabricating gas-tight 1–2 μm thick 8YSZ electrolyte layers on a regular NiO/8YSZ substrate, with a rough surface, a high porosity and a large pore size. These layers were deposited in a similar way as conventional suspension based layers, but the essential difference includes the use of coating liquids (nano-dispersion, sol) with a considerably smaller particle size (85 nm, 60 nm, 35 nm, 6 nm). Successful deposition of such layers was accomplished by means of an innovative coating process, which involves the preparation of a hybrid polyvinyl alcohol/8YSZ membrane by dip-coating or spin-coating and subsequently burning out the polymer part at 500 °C. Results from He leak tests confirmed that the sintered layers posses a very low number of defects and with values in the range $10^{-4}$–$10^{-6}$ (hPa dm$^3$)/(s cm$^2$) the gas-tightness of the thin film layers is satisfactory for fuel cell operation. Moreover, preliminary results have also indicated a potential reduction of the sintering temperature from 1400 °C to the range 1200–1300 °C, using the presented coating process.


*Keywords:* Fuel cells; Films; $ZrO_2$; Sol–gel processes; Thin 8YSZ electrolyte

## 1. Introduction

The work described in this paper deals with the development of novel solid oxide fuel cells (SOFCs) with thin film 8YSZ electrolytes. Initially, SOFCs were often prepared with the electrolyte layer as supporting material. Of course, resistance losses were significant, because of the required large thickness of the electrolyte layer. More recently, by using the anode as the support, the mechanical stability of the cells has been transferred from the electrolyte to the anode. This enabled a reduction of the electrolyte thickness from ∼150 μm to ∼10 μm, which gives a decrease in ionic resistance by more than one order of magnitude across the electrolyte.[1–3]

The manufacturing of planar anode-supported SOFCs is now a state of the art technology in a number of institutes. In our institute, a manufacturing procedure for cells with a size of 20 cm × 20 cm and current density of ∼2 A/cm$^2$ at 800 °C and 700 mV is established (feed gas 3% $H_2O/H_2$). The basic components of our SOFC are a planar porous NiO/8YSZ support, a porous NiO/8YSZ anode functional layer (AFL), a dense 8YSZ electrolyte layer and a porous LSM or LSCF cathode. In the standard manufacturing procedures, the substrate is made by tape casting or warm pressing and, subsequently, the respective layers are deposited from a suspension by means of vacuum slip casting or by screen printing.[4,5] In Fig. 1, a SEM image of a typical cell with a conventional 8YSZ electrolyte layer with a thickness of ∼10 μm is shown.

Since the ion conductivity through the electrolyte membrane is inversely proportional to the layer thickness, further reducing the thickness would significantly improve the power density and allow a reduction of the cell operating temperature to the range 600–700 °C or even lower.[6] An important consideration is that material compatibility and sealing problems would also be much simpler.[7] However, for the deposition of layers with a thickness below ∼5 μm and a satisfactory gas-tightness, conventional powder coating methods are no longer applicable.

* Corresponding author. Tel.: +49 2461 615443; fax: +49 2461 612455.
*E-mail address:* t.van.gestel@fz-juelich.de (T. Van Gestel).

0955-2219/$ – see front matter © 2011 Elsevier Ltd. All rights reserved.
doi:10.1016/j.jeurceramsoc.2011.07.012

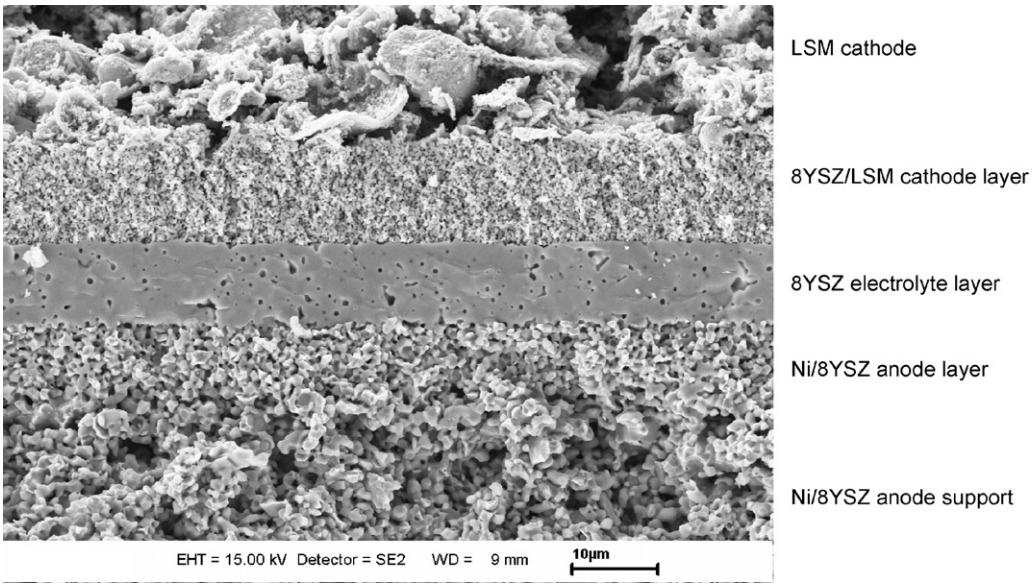


Fig. 1. SEM micrograph of a conventional SOFC prepared at FZJ, with Ni/8YSZ anode support, Ni/8YSZ AFL, 8YSZ electrolyte layer, 8YSZ/LSM cathode layer and LSM cathode (bar = 10 μm).

In the literature, a number of thin film deposition methods have already been proposed, including wet coating methods like sol–gel dip-coating and spin-coating[6,8] and particularly pulsed laser deposition (PLD), physical vapour deposition (PVD) and chemical vapour deposition (CVD).[9–15] The deposition processes are however frequently carried out on dense substrates such as Si-wafers or sapphire substrates or specially designed porous substrates rather than practical porous electrodes.

The purpose of our research was to study the deposition of thin film 8YSZ electrolyte layers on a regular SOFC substrate, consisting of anode support and anode functional layer (AFL), which is characterized by a relatively rough surface, a high porosity and a large pore size. In our institute, two types of planar NiO/8YSZ anode supports are fabricated. The first type is made by a warm pressing procedure (Coat mix©) and has been frequently used for making larger stacks, which are composed of 20 cm × 20 cm plates (sintering at 1400 °C). The second type is made by a tape casting method, which gives a thinner and also smoother support material.[16] The experimental work in this paper was done with the warm pressed support, which is the most difficult material, in terms of surface roughness. Transfer of the developed thin film electrolytes to the smoother tape casted support has been experienced as unproblematic and is therefore not specifically reported in this paper.

First results of our research on the preparation of thin film 8YSZ electrolytes on SOFC substrates were already reported previously.[17] The main conclusion of the work was that a coating liquid with a relatively large particle size is required, for the deposition of a homogeneous non-infiltrated layer. Included in that work was the deposition of 2–3 μm thick layers by a dip-coating technique, using an 8YSZ dispersion with a particle size of ∼200 nm in light-scattering measurements. Complete sintering of the layer was obtained at 1400 °C, which is also the same temperature at which the conventional 8YSZ electrolyte layer is fired. SEM images taken after firing at a reduced temperature of 1200–1300 °C showed very porous layers. Another limitation of the previous work included a relatively small sample size (3 cm × 3 cm – 4 cm × 4 cm) and the gas-tightness was not yet accurately determined.

In this article, a more comprehensive study of the deposition of 8YSZ thin film electrolyte layers is presented. Various nano-dispersion and sol coating processes are reported, with an average particle size of 85 nm, 60 nm, 35 nm and 6 nm in light-scattering. Compared with the previous dispersion coating process, these coating liquids were expected to form even thinner precursor layers with a significantly smaller pore size. Techniques used for coating include dip- and spin-coating, which are established wet coating techniques with a potential for large scale production. Further densification of the developed fine porous precursor layers is studied systematically in the range 1200–1400 °C. In the last part of this article, the gas-tightness of thin film 8YSZ layers, deposited on 7.5 cm × 7.5 cm anode substrates, is evaluated. Continuing work on the development and electrochemical characterization of complete cells is ongoing and will be presented in a later publication. A first short-term test result of a cell, which contains one of the layers developed in this work and the same LSCF cathode and CGO Sr-diffusion barrier layer as in our regular SOFC, has been published very recently elsewhere.[18]

## 2. Experimental

### 2.1. Anode substrate

The substrate preparation method includes a warm pressing method (Coat mix©) to prepare the support plate and subsequently the anode functional layer (AFL) is coated by vacuum slip casting. In both steps, commercial NiO (Mallinckrodt Baker) and 8YSZ powders (Support: Unitec Ceramics, AFL:

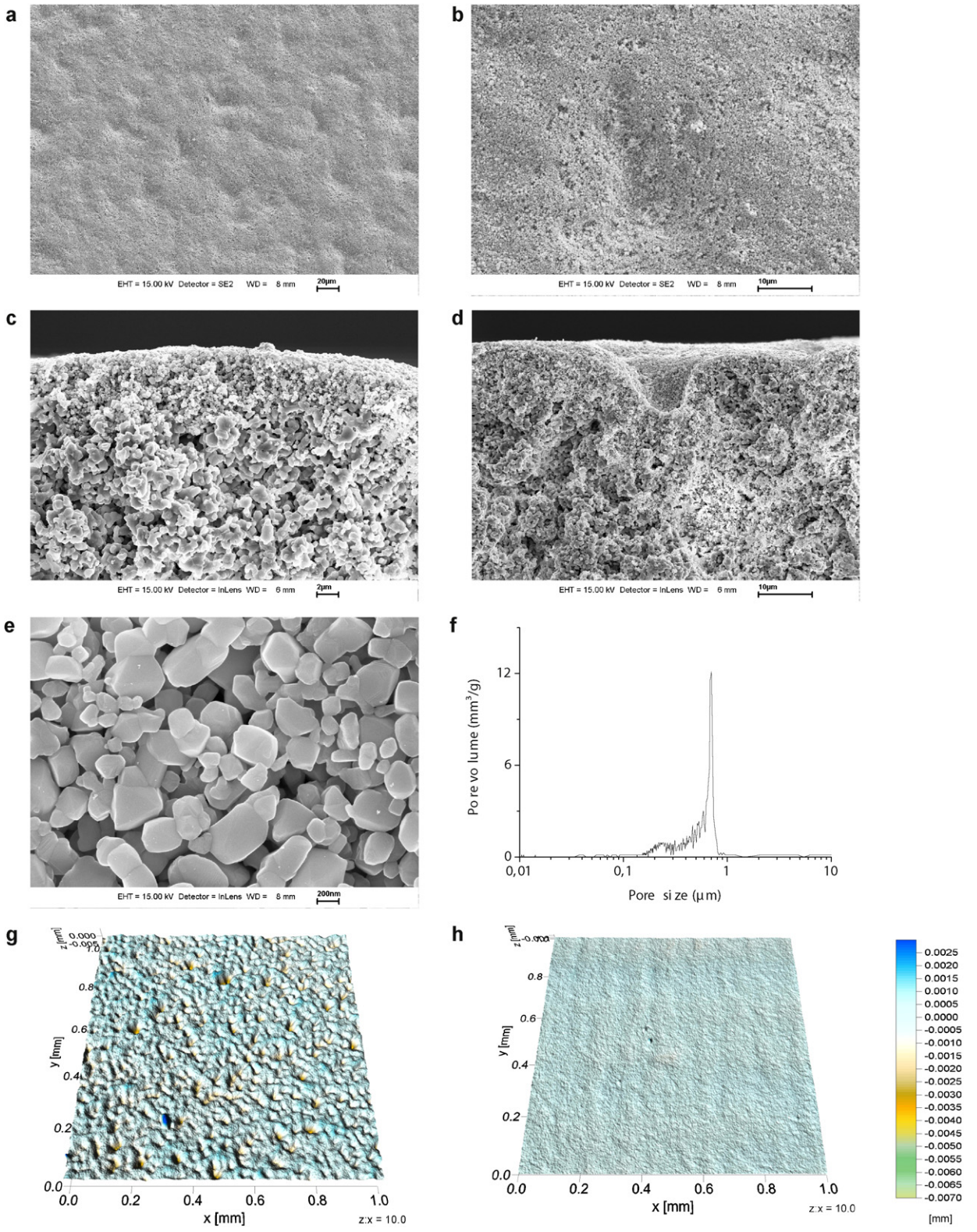


Fig. 2. Characterization of the anode substrate: (a) surface image; (b) surface micrograph, showing surface roughness; (c) fracture micrograph showing the anode support and the AFL; (d) fracture micrograph showing a strongly curved area; (e) high-magnification surface micrograph of the AFL; (f) pore size distribution; (g) surface profile of a warm pressed substrate (area 1 mm × 1 mm); (h) surface profile of a tape casted substrate (area 1 mm × 1 mm).

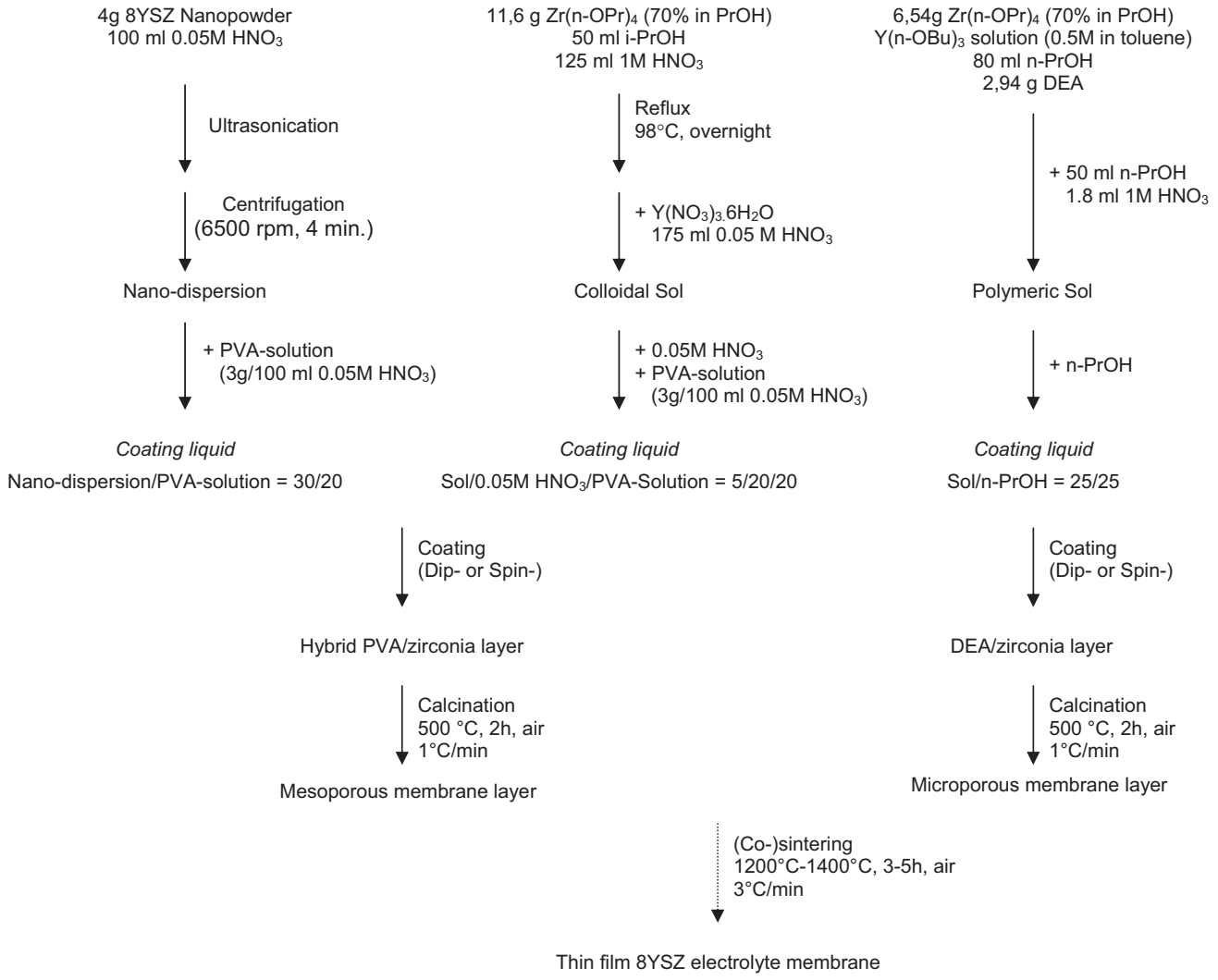


Fig. 3. Schematic overview of the different preparation routes of porous 8YSZ precursor membrane layers. In route 1, a nano-dispersion is prepared and deposited by dip-coating or spin-coating. The deposition of additional sol–gel layers is carried out according to route 2 and 3. (Co-)sintering is carried out after the deposition of the respective layers.

Tosoh) are used. Presintering of the support plate is done at 1230 °C for 3 h; the AFL is presintered at 1000 °C for 2 h.

The finished anode substrate has a dimension of ~25 cm × 25 cm and a thickness of 1 mm or 1.5 mm. The morphology of the substrate surface is visualized in Fig. 2. Basically, in both SEM (Zeiss Ultra) and 3D-profilometry (Cybertechnologies CT 350S), the surface shows a significant roughness, characterized by strongly curved areas. Roughness data in Table 1 of 3 different 7.5 cm × 7.5 cm substrates, which were cut from the same 25 cm × 25 cm plate, confirm this. It is assumed that the roughness stems from the press-forms in the manufacturing step of the support. In micrograph Fig. 2c and d, it can be seen that the AFL is ~4–6 μm thick and the thin AFL appears to follow the waviness of the support plate. In micrograph Fig. 2e, a typical macroporous structure can be recognized for the AFL, with a particle size of 200–400 nm and an average pore size of 200–300 nm. The pore size distribution in Fig. 2f shows a pore size of ~0.7 μm for the support plate (large peak) and a comparable pore size of ~200–300 nm for the AFL (small peak). For comparison, surface data of a smoother tape-casted substrate (thickness ~0.5 mm) with an AFL made by screen-printing are also given (Table 1, Fig. 2h).

### 2.2. Preparation of the coating liquids

The preparation routes of the different coating liquids are schematically summarized in Fig. 3. Coating liquid 1 was a nano-dispersion, made by dispersing a commercial 8YSZ nanopowder

Table 1
Surface roughness data of anode substrates described in the text (support plate + AFL).

| Substrate | $R_a$ (μm) | $R_q$ (μm) | $R_z$ (μm) | $R_{max}$ (μm) |
|---|---|---|---|---|
| Warm pressed S1 | 0.508 | 0.665 | 3.667 | 4.846 |
| Warm pressed S2 | 0.613 | 0.783 | 4.125 | 5.239 |
| Warm pressed S3 | 0.519 | 0.678 | 3.837 | 5.209 |
| Tape casted S1 | 0.218 | 0.276 | 1.379 | 2.253 |
| Tape casted S2 | 0.140 | 0.181 | 1.016 | 1.613 |
| Tape casted S3 | 0.199 | 0.251 | 1.199 | 1.664 |

S1, S2, S3: sample 1, sample 2, sample 3.

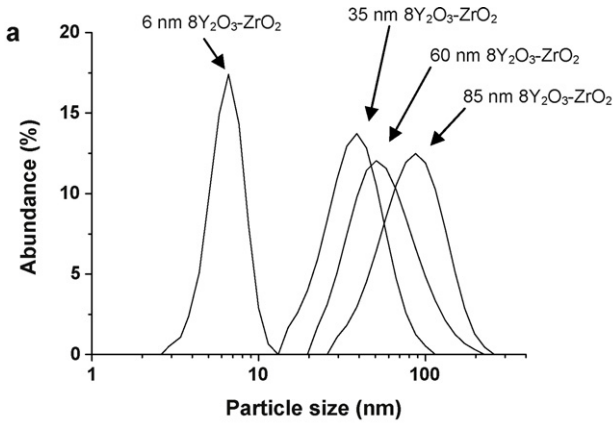


Fig. 4. (a) Particle size distribution of the different coating liquids used in this work. (b) Coating liquids: (1) 85 nm nano-dispersion; (2) 60 nm nano-dispersion; (3) 35 nm colloidal sol; (4) 6 nm polymeric sol.

(Evonik) in a 0.05 M aqueous $HNO_3$ solution by ultrasonication and subsequent separation of larger agglomerates by centrifugation. As shown in Fig. 4a, characterization of the particle size gives an average size of ~85 nm and the appearance of the liquid was opaque. Coating liquid 2 was a nano-dispersion with a smaller particle size of ~60 nm, which was made with a nanopowder supplied by Sigma–Aldrich. As shown in Fig. 4b, this coating liquid was translucent.

Coating liquids 3 and 4 are different from the previous liquids, since they are made by a chemical synthesis method, starting from a metal-organic compound. All chemicals were obtained from Sigma–Aldrich. The colloidal particle sol method involves the formation of zirconia particles, starting from $Zr(n\text{-}OC_3H_7)_4$ in an isopropanol–water–$HNO_3$ solution at 98 °C. Yttria-doping (8 mol% $Y_2O_3$) is done by adding the proper amount of $Y(NO_3)_3{\cdot}6H_2O$ to the finished zirconia sol. In this synthesis procedure, the size of the colloidal particles in the sol is controlled by controlling the time of the aging process and the best sol coating results are obtained for particles with an average size of ~30–40 nm. The fourth coating liquid was a nanoparticle 8YSZ sol. This sol was synthesized by controlled hydrolysis of $Zr(n\text{-}OC_3H_7)_4$, in the presence of diethanol amine (DEA) as a precursor modifier/polymerization inhibitor and

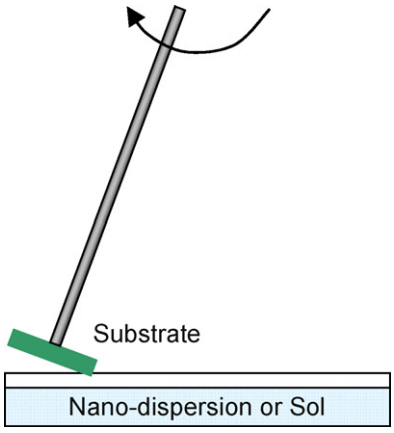


Fig. 5. Schematic representation of the rotary dip-coating technique used in this work.

an yttrium precursor $Y(OC_4H_9)_3$ as a doping compound. The ratio [Zr]/[DEA] was 2, which gives a reproducible formation of particles with a size of ~5 nm in light-scattering.[19]

As can be seen in Fig. 4b, the polymeric sol with the smallest particle size appears completely transparent and the opacity of the liquids increases with increasing particle size going from the 35 nm sol over the 60 nm nano-dispersion to the 85 nm nano-dispersion. It should be noted that the names nano-dispersion, colloidal sol and polymeric sol have been chosen based on the terminology frequently used in the literature. Strictly spoken, each coating liquid in this work is a sol or colloidal suspension, since a sol is defined as a colloidal suspension of solid particles in a liquid, in which the dispersed phase is small enough so that gravitational forces can be neglected.[20]

The particle size distribution of the nano-dispersions and sols was measured with a dynamic laser beam scattering method (Horiba LB-550). Additional characterization of the particles in the different liquids was also done by TEM (Fei, Tecnai G2 F20, 200 kV). The liquids were applied on a copper grid with an electron beam transparant graphite layer.

### 2.3. Membrane coating

To deposit a thin film 8YSZ layer, dip-coating or spin-coating was applied. Dip-coating was done with a lab-scale automatic dip-coating device, which is equipped with a rotary arm with a rubber vacuum chuck (KSV NIMA). The chuck was connected to a pump to hold the anode substrate during the coating process. In order to obtain a membrane film of 8YSZ particles on the AFL side of the substrate, dipping was performed as shown in Fig. 5 in such a way that solely the AFL side was immersed. To prevent strong infiltration of the 8YSZ particles during the coating step, polyvinyl alcohol was added to the coating liquid (PVA, Merck, 60,000 g/mol). As could be seen from the dried coating liquids, PVA forms a hybrid polymeric membrane layer with the 8YSZ nanoparticles distributed in it, thus preventing infiltration of the nanoparticles during the coating step. Due to the smaller size of our dip-coater, the size of the samples was limited to 5 cm × 5 cm in the dip-coating method.

After the coating step, the substrate was fired in a conventional furnace at 500 °C in air. Removal of the organic additives results in a meso- or microporous material with a pore size of ∼15 nm, 6–7 nm, 3–4 nm and <1 nm, dependent on the size of the 8YSZ particles.[21] Unless stated otherwise, the coating and calcination step was repeated once for each coating liquid and, for graded multilayer coatings, the same procedure was additionally repeated with a smaller particle size. Finally, the porous precursor 8YSZ layer was sintered at a temperature of 1400 °C, 1300 °C or 1200 °C. Characterization of the 8YSZ membrane layers during the different preparation steps was done by FEG-SEM (Zeiss Ultra 55). This included (1) breaking the original sample into a piece of approximately 1 $cm^2$, (2) mounting it on a conventional sample holder for surface or fracture surface SEM images, (3) sputtering an approximately 2 nm thick Pt layer, and (4) applying a conductive copper tape.

In the second part of this work, selected coating liquids and combinations of coating liquids were spin-coated (Süss MicroTec D80T2) and the gas-tightness of the sintered samples was tested with a He leak tester. A typical coating step involved dropping 10 ml of the coating liquid onto an anode substrate with a size of 7.5 cm × 7.5 cm, which was hold by a vacuum chuck, and spinning the substrate at 800–1200 rpm during 1 min. For coating, the same liquids were used as in the dip-coating experiments and the spin-coated layers were also calcined and sintered in the same way. The He leak rate was measured as follows. First, the coated substrate was placed with the 8YSZ layer side on the sealing (test area 4 cm × 4 cm) and a vacuum was installed. Then, He was supplied to the module until a constant flow was obtained. Analysis of the leak stream was done with a mass spectrometer (HLT 260, Pfeiffer Vakuum). It should be noted that the threshold specific He leakage for conventional electrolyte layers is set at $2 \times 10^{-5}$ (hPa $dm^3$)/(s $cm^2$) in our institute. This specific He leakage is normalised to the measuring area and to a pressure difference of 100 hPa, which is typical for an SOFC stack.

## 3. Results

### 3.1. Characterization of the coating liquids

The particle size distributions and the appearance of the coating liquids were already discussed in the experimental part. In TEM images, it appeared that the observed larger particles in the coating liquids are in fact agglomerates of smaller primary particles. TEM images Fig. 6a and b of the 85 nm and 60 nm nano-dispersion show spherical crystalline primary particles with a size of ∼5 nm. TEM images of the 35 nm and 6 nm sols in 6c and 6e show no well-defined structures and it is impossible to determine the particle shape or size. After calcination, the amorphous material crystallized as shown in 6d and 6f and TEM showed similar images as previously found for the nano-dispersions, in particular for the colloidal type of sol. The polymeric sol procedure yielded also spherical primary particles, but here the size was clearly below 5 nm.

### 3.2. Coating of the 8YSZ electrolyte layers

#### 3.2.1. 85 nm nano-dispersion

Micrographs Fig. 7a and b show a mesoporous 8YSZ precursor layer, which was obtained by coating with the 85 nm nano-dispersion and firing at 500 °C. These images were made in the back-scatter mode, which gives an improved contrast between layers with a different pore size or porosity. Under a low magnification, the anode support plate, the AFL and the mesoporous 8YSZ precursor layer can be clearly recognized and the latter layer is also clearly visible as a brighter film, due to its much smaller pore size (Fig. 7a). In Fig. 7b, it is confirmed that infiltration of 8YSZ particles into the macropores of the AFL could be prevented. Here, a kind of separation line is also visible in the 8YSZ layer, which marks an area with a higher concentration of particles at the separation between the first and second layer. Further, it appears that a thickness of ∼2 μm was obtained for a single layer, made by one coating-calcination step.

Densification of the precursor layer during further firing is shown in micrographs Fig. 7c–h. From the high-magnification fracture and surface micrographs Fig. 7c and d, taken after firing at 1300 °C, it seemed that a dense homogeneous layer with a grain size of ∼1 μm was obtained. Under a lower magnification, however, a number of very untight areas were observed and apparently the layer was only partly densified (Fig. 7e). After firing at 1400 °C, on the other hand, a fully densified layer was obtained. The surface micrograph Fig. 7g shows that such a layer is composed of comparatively large grains, with a size up to 2 μm and larger. Since the fracture micrograph Fig. 7f shows a layer thickness of ∼2 μm, this implies that some of the grains should have a flattened shape – with a width that exceeds the thickness of the grain – rather than a round shape. Sintering of the AFL as observed in Fig. 7f is also obtained in our standard manufacturing process. In fact, the layer is only partially sintered and the required anode porosity for cell operation is also afterwards obtained, when NiO is reduced to metallic Ni during operation in reduced atmosphere.

#### 3.2.2. 85 nm nano-dispersion + 60 nm nano-dispersion + 35 nm colloidal sol

Since a larger particle size is helpful for the formation of a continuous layer on the very porous substrate, while a smaller particle size is expected to improve the sintering process, further experiments with layers with a reduced particle and pore size were carried out. In a first experiment, the 85 nm nano-dispersion was coated as described in the previous section and then an additional layer was coated with the 60 nm nano-dispersion. As can be seen in micrograph Fig. 8a, this layer shows a smaller thickness of ∼1 μm and also a smaller pore size, based on the brighter appearance in the back-scatter image. Comparison of high-magnification surface micrographs of a layer made from an 85 nm (Fig. 9a) and a 60 nm (Fig. 9b) nano-dispersion confirmed also that finer 8YSZ particles give a layer with a smaller pore size. For comparison, a layer made from a 35 nm (Fig. 9c) and 6 nm sol (Fig. 9d) are also shown.

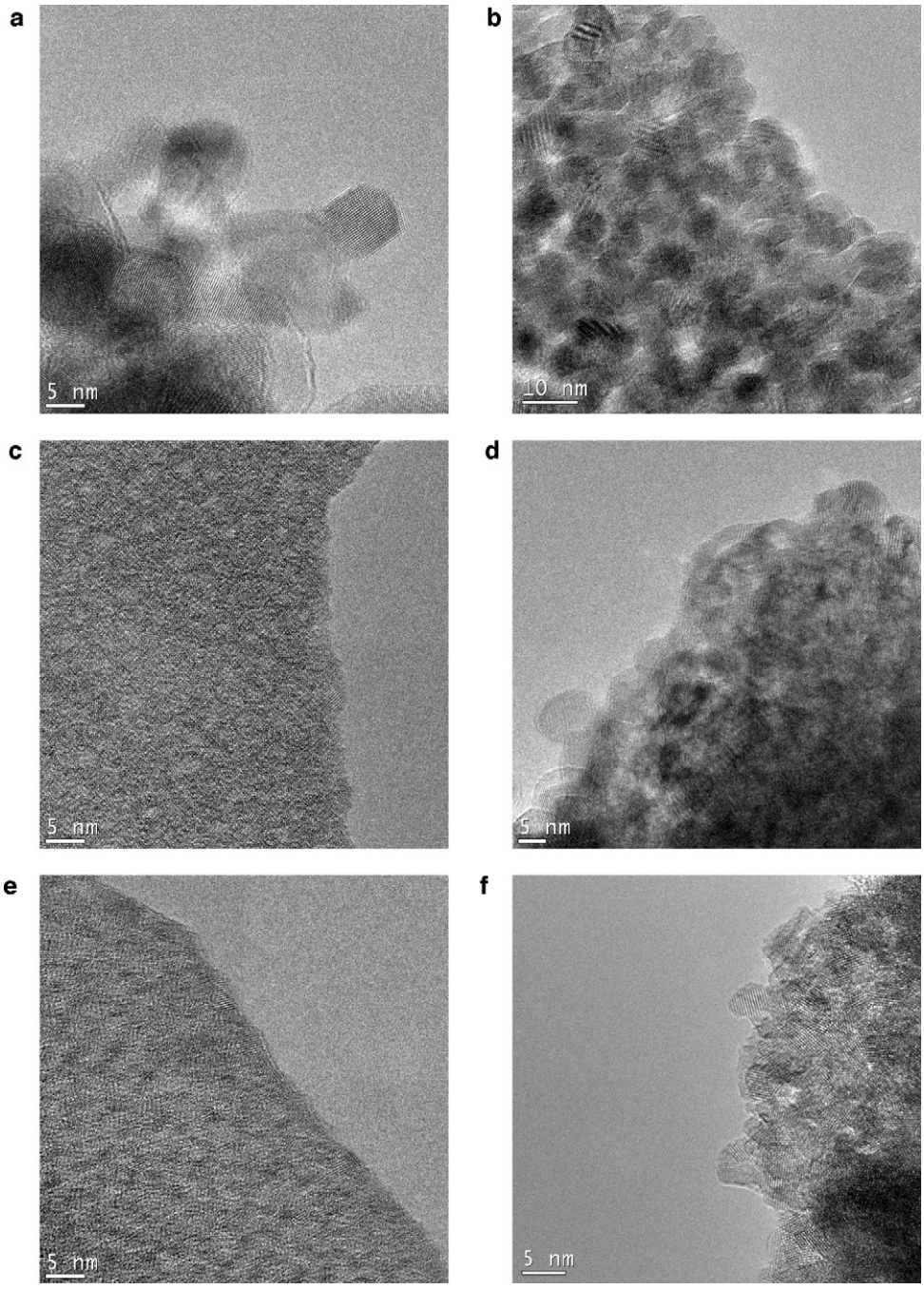


Fig. 6. TEM micrographs of the coating liquids: (a) 85 nm nano-dispersion; (b) 60 nm nano-dispersion; (c) 35 nm colloidal sol; (d) colloidal sol after firing at 500 °C; (e) 6 nm polymeric sol; (f) polymeric sol after firing at 500 °C.

In the detail micrographs Fig. 8b and c, taken after firing at 1200 °C, a thin dense 8YSZ layer with a grain size of a few hundred nanometers can be seen. In Fig. 8b, it appears that the 85 nm nano-dispersion layers sintered only partially, while the layer made from the 60 nm nano-dispersion looks dense. However, low-magnification micrographs showed a number of untight areas, particularly where the substrate surface is strongly curved, as shown in Fig. 8d. At 1300 °C, an increase in grain size to the micrometer range was obtained (Fig. 8e), but also here a similar untight layer was observed (Fig. 8f). Micrographs taken after firing at 1400 °C indicated, in analogy with the 85 nm nano-dispersion coating experiment in the previous section, a fully densified layer with a thickness of ~2 μm (Fig. 8g and h)

In another coating experiment, a graded mesoporous 8YSZ precursor layer was made, by coating subsequently with the 85 nm and the 60 nm nano-dispersion and in addition the 35 nm colloidal sol. Micrograph Fig. 10a shows a back-scatter image of such a layer combination, with the different nano-dispersion layers and a double-coated colloidal sol layer. Here, after

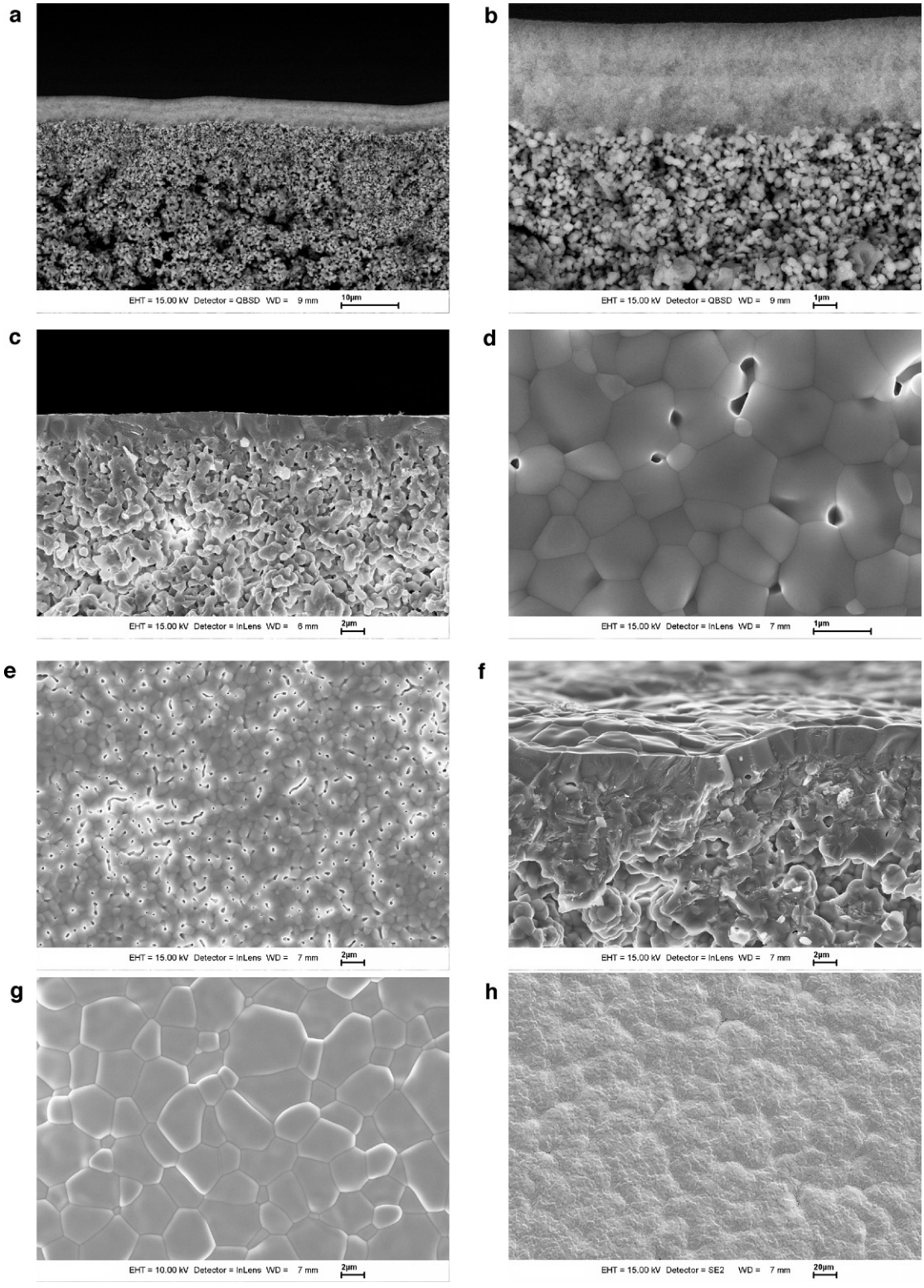


Fig. 7. (a and b) Mesoporous precursor layer, obtained by dip-coating the 85 nm nano-dispersion (2 coating steps, firing at 500 °C). (c–e) After firing at 1300 °C. (f–h) After firing at 1400 °C. ((a) bar = 10 μm, (b and d) bar = 1 μm, (c, e, f, and g) bar = 2 μm, (h) bar = 20 μm).

firing at 1200 °C, the 60 nm nano-dispersion and sol layers co-sintered into a layer with a thickness <1 μm (Fig. 10b), in which however scattered some pores and untight areas were present (Fig. 10c). After firing at 1300 °C and 1400 °C, fully densified layers with a thickness of ~2 μm can be observed (Fig. 10d–h) and, in contrast with the previous experiments, no untight areas are present in the low-magnification images of the layer fired at 1300 °C (Fig. 10e and f).

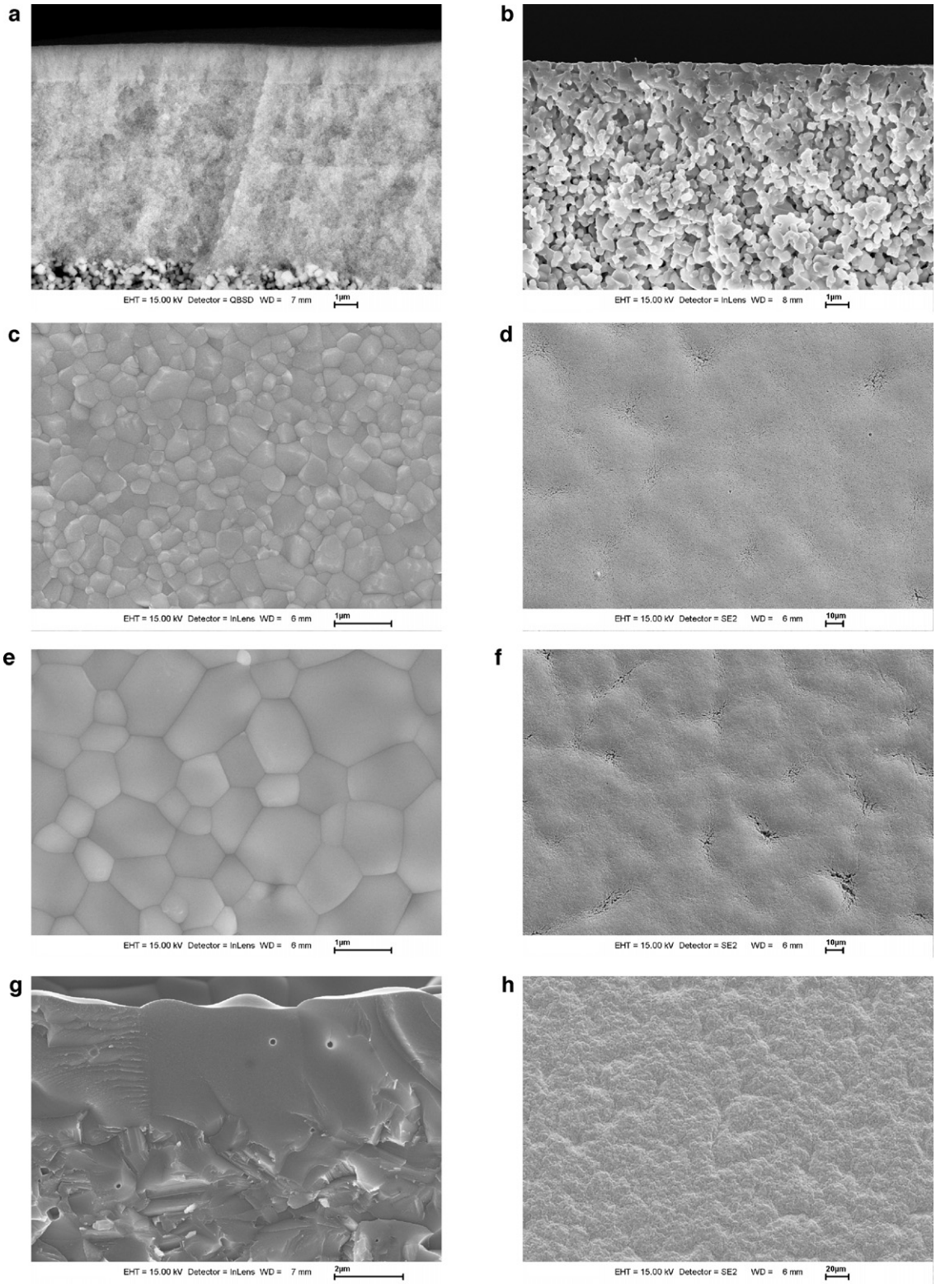


Fig. 8. (a) Mesoporous precursor layer, obtained by dip-coating subsequently the 85 nm and 60 nm nano-dispersion (85 nm liquid: 2 coating steps, 60 nm liquid: 1 coating step, firing at 500 °C). (b–d) After firing at 1200 °C. (e–f) After firing at 1300 °C. (g–h) After firing at 1400 °C. ((a, b, c, and e) bar = 1 μm, (d and f) bar = 10 μm, (g) bar = 2 μm, (h) bar = 20 μm).

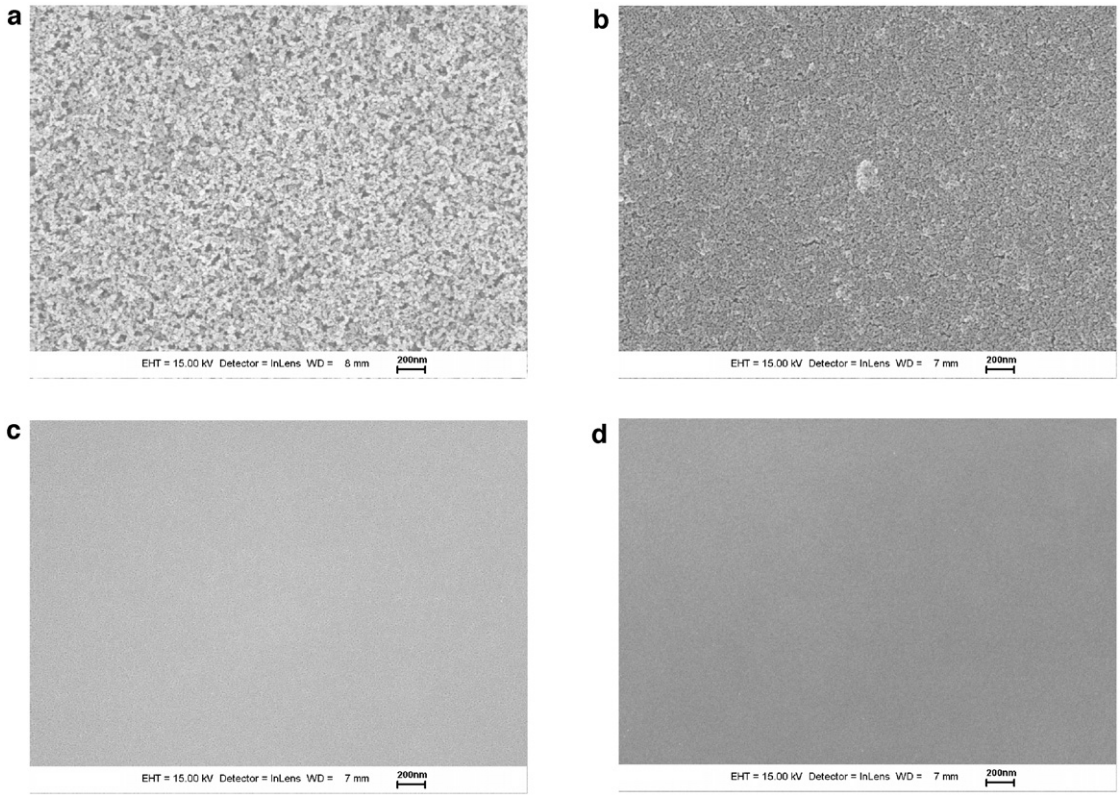


Fig. 9. Comparison of the surface of calcined layers, obtained by dip-coating the 85 nm nano-dispersion (a), the 60 nm nano-dispersion (b), the 35 nm colloidal sol (c) and the 6 nm polymeric sol (d) (bar = 200 nm).

### 3.2.3. 60 nm nano-dispersion

Micrographs Fig. 11a and b shows back-scatter images of a mesoporous precursor layer prepared by coating twice the 60 nm nano-dispersion. Infiltration of the smaller 8YSZ particles into the pores of the AFL could also be prevented here and a very homogeneous membrane layer with a single layer thickness of ∼1 μm was obtained.

Further firing at 1200 °C resulted in a ∼1 μm thick 8YSZ layer with a grain size of a few hundred nanometers (Fig. 11c and d). The layer looks well-sintered and tight in the fracture micrographs, but a significant number of pores are evident in the low-magnification surface micrograph Fig. 11e. After firing at 1300 °C, a ∼1 μm thick 8YSZ layer with an increased grain size of ∼1 μm was observed (Fig. 11f–h). Under high magnification, it appears also here that the thickness of the layer equals exactly one single grain (Fig. 11g). Further, from low-magnification micrographs it is clear that densification had proceeded to a much larger extent, compared with the 85 nm nano-dispersion coating experiment in Section 3.2.1. The problem of untight areas in the 8YSZ layer, which are present in areas where the surface profile shows a strong curvature, is however also observed in low-magnification micrographs (Fig. 11j and k). At 1400 °C, these untight areas disappeared again and a dense layer with a thickness of ∼1 μm is observed (Fig. 11l–p). As can be seen in micrographs Fig. 11m–o, grains with a width that exceeds the layer thickness are also here obtained.

### 3.2.4. 60 nm nano-dispersion + 35 nm colloidal sol + 6 nm polymeric sol

Based on the previous mesoporous layer, graded precursor layers with even finer layers were further investigated. In a first test, the 35 nm colloidal sol was coated twice on the previously deposited 60 nm nano-dispersion layer, which gave an additional layer with an overall thickness of ∼0.5 μm and a significantly smaller pore size (Fig. 12a). In a previous article, where similar materials were studied for the formation of porous ceramic gas separation membranes, a pore size of 6–7 nm and 3–4 nm was reported for the respective materials made from the nano-dispersion and the colloidal sol.[21] Here, a reduction of the pore size could also be visually observed in the surface Fig. 9b and c.

After firing at 1200 °C, a similar thickness of ∼1 μm as in the previous coating experiment was obtained, which indicates that the additional sol–gel coating has a negligible influence on the layer thickness after sintering. According to the high-magnification fracture and surface Fig. 12b and c, the layer has also a comparable grain size of a few hundred nanometers. Further, in comparison with all the previous coating experiments, the application of this coating sequence resulted clearly in the highest degree of densification at 1200 °C, despite the fact that scattered pores and untight areas were found in low-magnification micrographs (e.g. Fig. 12d). It should however also be noted that the roughness of this sample (e.g. in Fig. 12e) appeared smoother than other samples in some of the previous

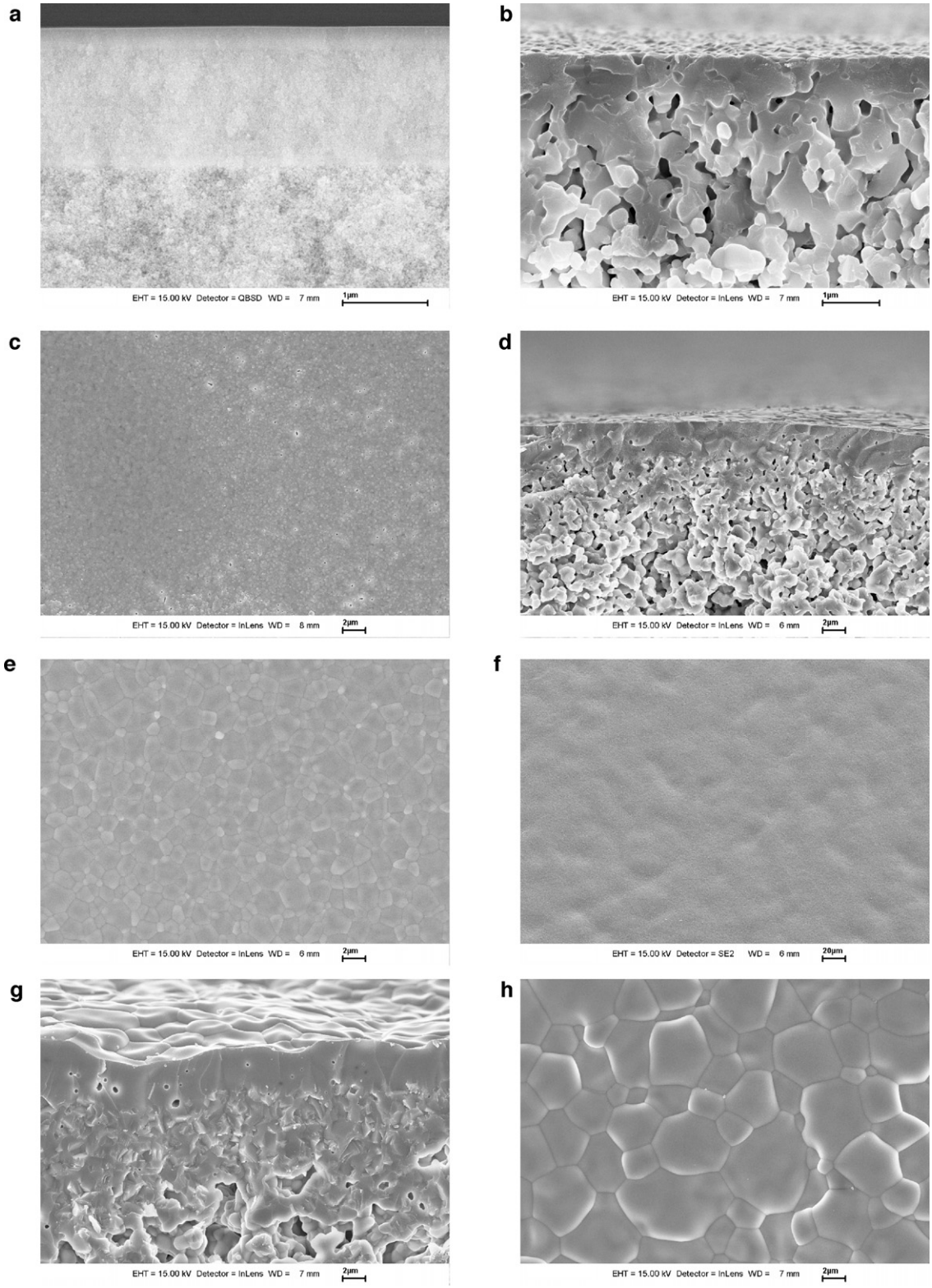


Fig. 10. (a) Mesoporous precursor layer, obtained by dip-coating subsequently the 85 nm and 60 nm nano-dispersion and the 35 nm colloidal sol (2 coating steps, firing at 500 °C). (b and c) After firing at 1200 °C. (d–f) After firing at 1300 °C. (g and h) After firing at 1400 °C. ((a and b) bar = 1 μm, (c, d, e, g, and h) bar = 2 μm, (f) bar = 20 μm).

experiments, which suggested a possible influence of the substrate surface morphology. After firing at 1300 °C, a dense layer with an increased grain size of ∼1 μm and a few scattered pores was obtained (Fig. 12f). The layer fired at 1400 °C showed a further increased grain size and a thickness of ∼1 μm and was completely dense (Fig. 12g and h).

A graded precursor layer with an additional finer toplayer was also made, by coating successively the 60 nm nano-dispersion,

the 35 nm colloidal sol and the 6 nm polymeric sol twice. Fig. 13a shows a similar graded structure as in Fig. 12a, with an additional thin layer obtained from the polymeric sol, with an estimated thickness of 100 nm. In micrograph Fig. 13b, a grain size of 100–200 nm can be estimated after firing at 1200 °C, but a few larger grains are also clearly present. Further, in the low-magnification surface micrograph Fig. 13c, no untight areas are visible. After firing at 1300 °C and 1400 °C, a 1 μm thick 8YSZ layer with a comparably increased grain size as in the previous examples can be observed.

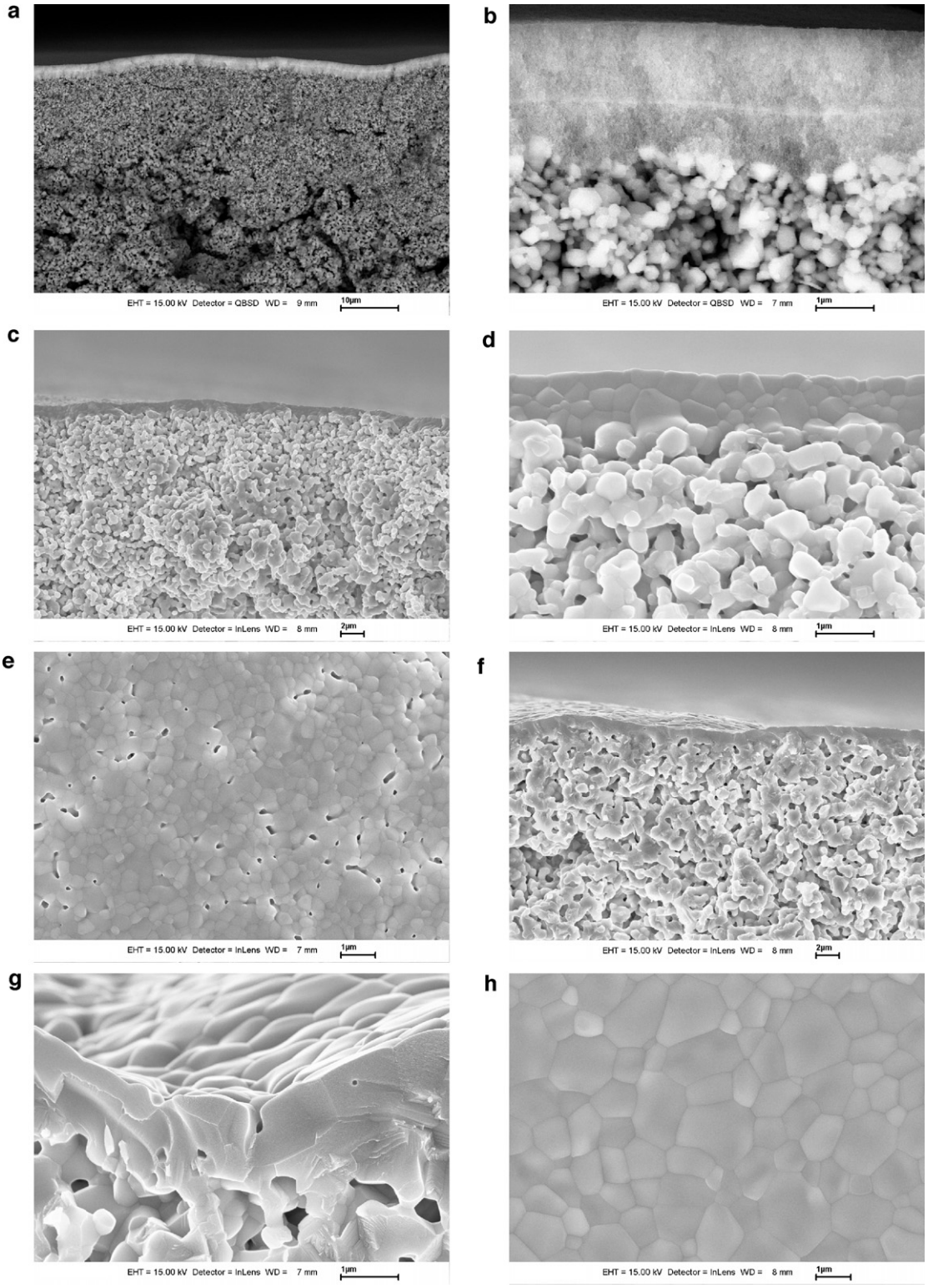


Fig. 11. (a and b) Mesoporous precursor layer, obtained by dip-coating the 60 nm nano-dispersion (2 coating steps, firing at 500 °C). (c–e) After firing at 1200 °C. (f–k) After firing at 1300 °C. (l–p) After firing at 1400 °C. ((a) bar = 10 μm, (b, d, e, g, h, and m) bar = 1 μm, (c, f, i, k, l, n, and o) bar = 2 μm, (j and p) bar = 20 μm).

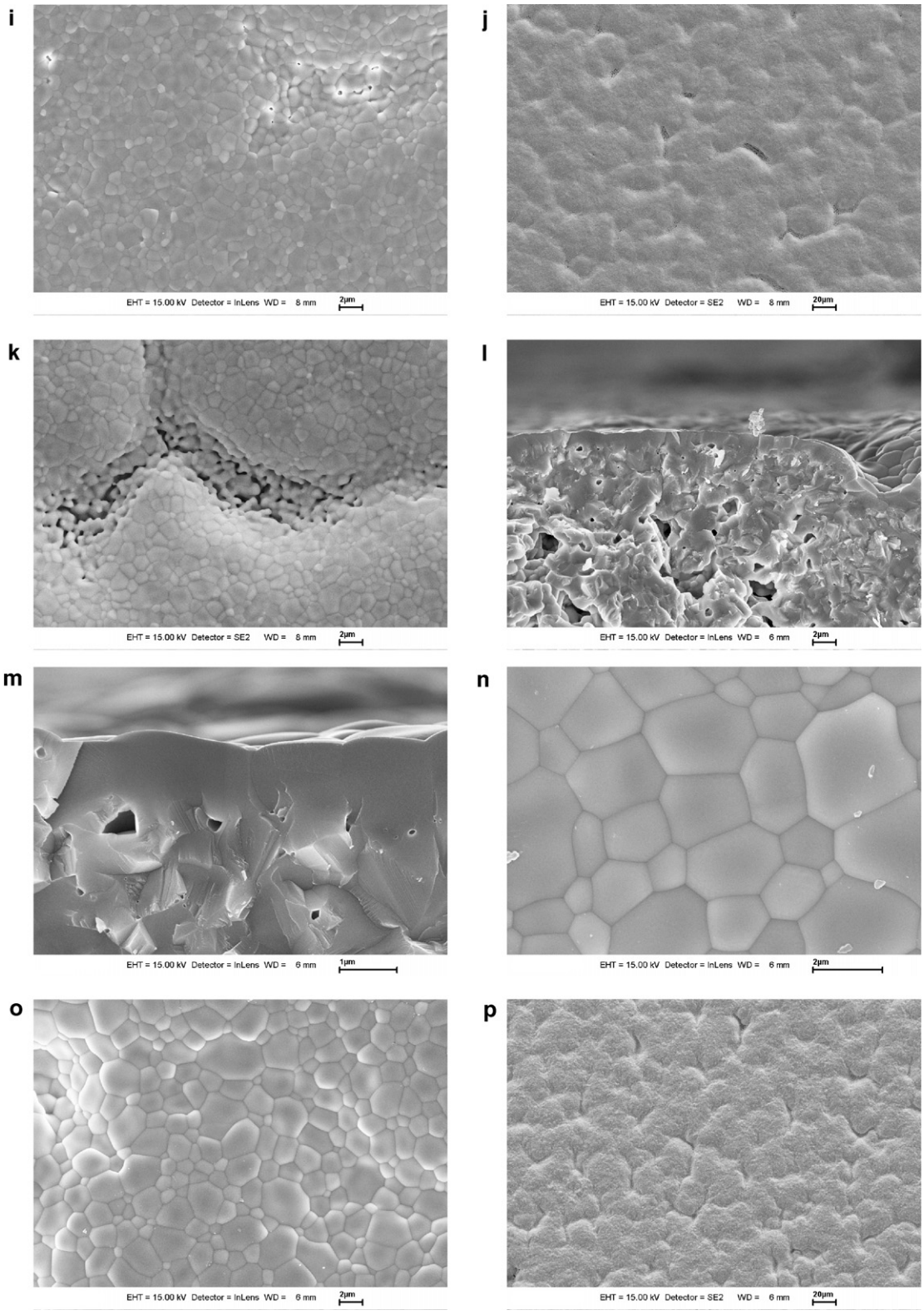


Fig. 11. (*Continued*).

### 3.3. Spin-coating experiments + He leak tests

A matching series of spin-coating experiments was carried out with 7.5 cm × 7.5 cm anode substrates and the same coating liquids. Subsequently, the gas tightness of the sintered 8YSZ layers was tested as described in Section 2. The results of these tests (Table 2) were basically in agreement with the experimental results discussed in the previous sections. First, samples with

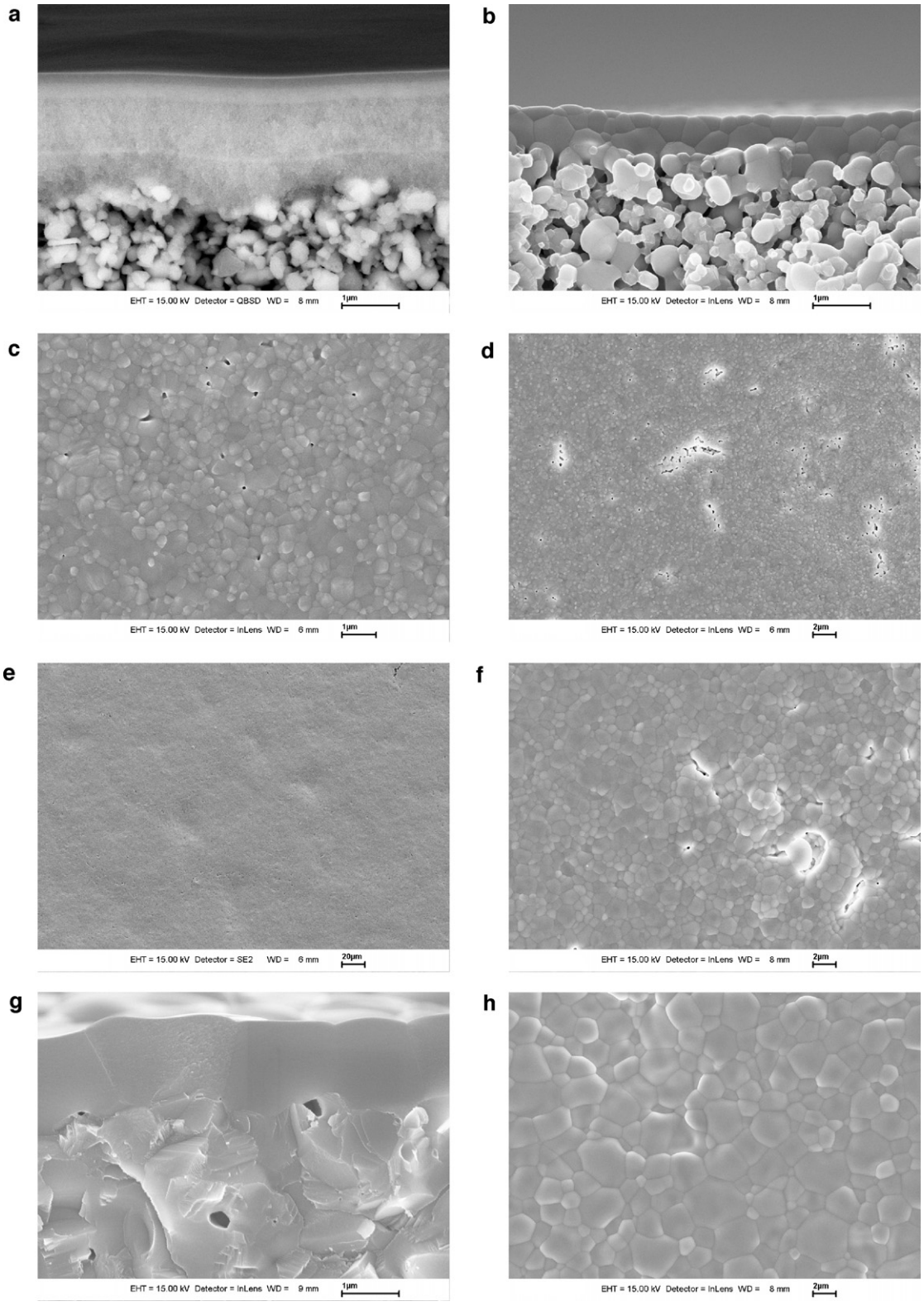


Fig. 12. (a) Mesoporous precursor layer, obtained by dip-coating subsequently the 60 nm nano-dispersion and the 35 nm colloidal sol (2 coating steps, firing at 500 °C). (b–e) After firing at 1200 °C. (f) After firing at 1300 °C. (g–h) After firing at 1400 °C. ((a, b, c, and g) bar = 1 μm, (d, f, and h) bar = 2 μm, (e) bar = 20 μm).

8YSZ layers made with the 85 nm (E1) or 60 nm (E2) nano-dispersion and sintered at 1400 °C looked very dense in SEM characterization and showed a comparable He leak rate with values in the range of $8 \times 10^{-4}$ to $1 \times 10^{-4}$ (hPa dm$^3$)/(s cm$^2$). This result confirmed that an effective coating process has been developed for the reproducible deposition of thin film 8YSZ electrolyte layers with a thickness of 1–2 μm, on a regular anode substrate.

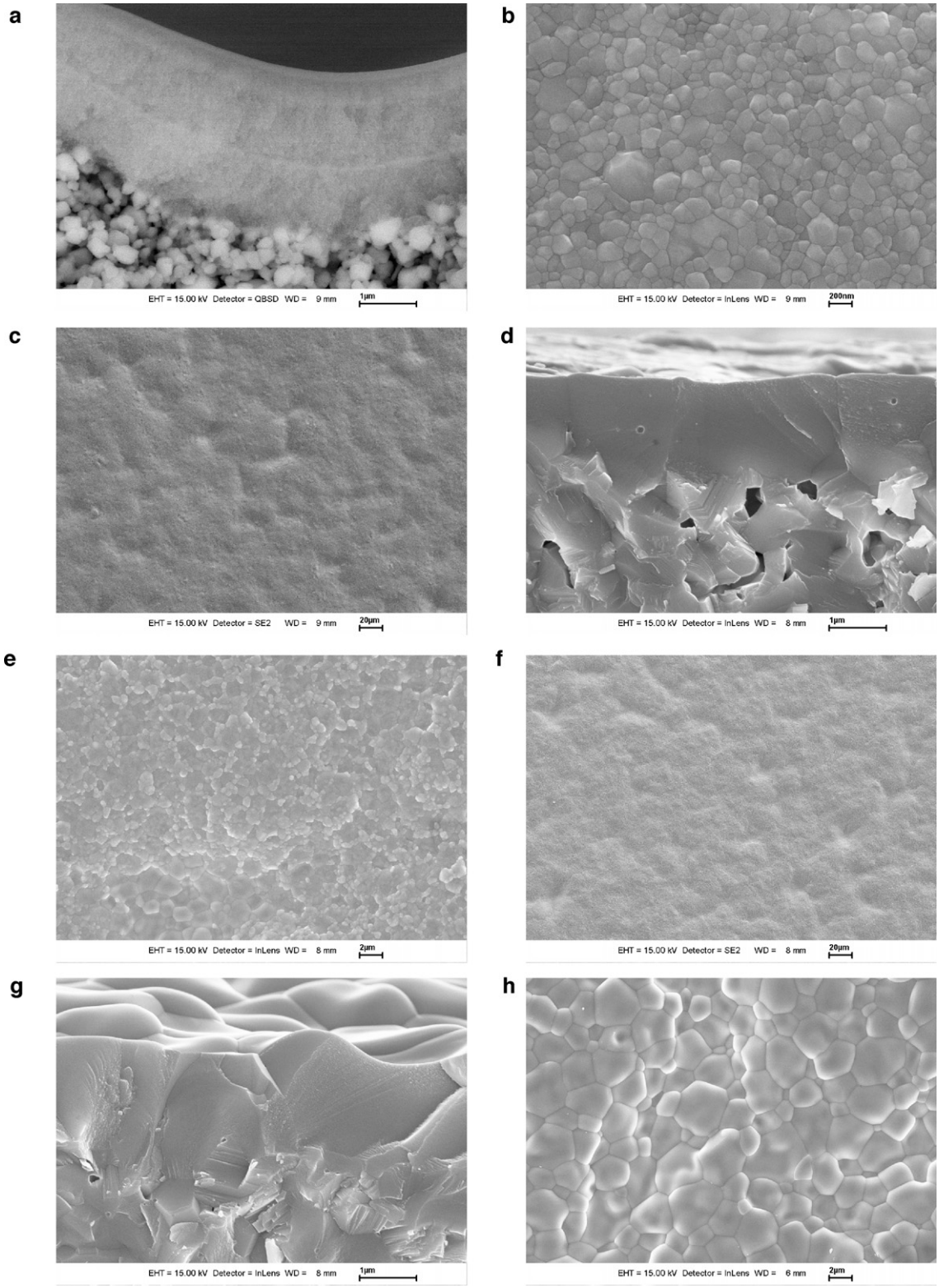


Fig. 13. (a) Precursor layer, obtained by dip-coating subsequently the 60 nm nano-dispersion and the 35 nm and 6 nm sol (2 coating steps, firing at 500 °C). (b and c) After firing at 1200 °C. (d–f) After firing at 1300 °C. (g and h) After firing at 1400 °C. ((a, d, and g) bar = 1 μm, (b) bar = 200 nm, (c and f) bar = 20 μm, (e and h) bar = 2 μm).

Samples obtained by coating subsequently the 60 nm nano-dispersion and 35 nm sol showed on average an improved leak rate (E3). Application of the 6 nm sol (E4–E5) showed in addition an improvement in the leak rate, but the effect is limited because the 100 nm thickness of the layer is probably too small to cause a large effect. The best leak rates were obtained for samples which comprise a first 85 nm nano-dispersion layer (E6), probably because the thickness of the final sintered electrolyte

Table 2
He leak test results of sintered 8YSZ thin film electrolyte layers, made by spin-coating.

| Sample | Coating liquid | Sintering temperature | Specific He leak rate (hPa dm$^3$)/(s cm$^2$) |
|---|---|---|---|
| E1a–E1e | 2 × 85 nm nano-dispersion | 1400 °C | 8.0E−04 |
| | | | 4.1E−04 |
| | | | 5.4E−04 |
| | | | 7.1E−04 |
| | | | 1.1E−04 |
| E2a–E2d | 2 × 65 nm nano-dispersion | 1400 °C | 6.2E−04 |
| | | | 2.0E−04 |
| | | | 5.4E−04 |
| | | | 1.4E−04 |
| E3a–E3g | 2 × 65 nm nano-dispersion | 1400 °C | 2.1E−04 |
| | +2 × 35 nm colloidal sol | | 3.1E−04 |
| | | | 6.7E−05 |
| | | | 9.7E−05 |
| | | | 9.3E−05 |
| | | | 5.9E−05 |
| | | | 1.3E−04 |
| E4a–E4f | 2 × 65 nm nano-dispersion | 1400 °C | 4.8E−05 |
| | +2 × 35 nm colloidal sol | | 1.4E−04 |
| | +2 × 6 nm polymeric Sol | | 5.2E−05 |
| | | | 5.5E−05 |
| | | | 3.6E−05 |
| | | | 2.0E−05 |
| E5a, E5b | 2 × 65 nm nano-dispersion | 1400 °C | 1.9E−04 |
| | +1 × 35 nm colloidal sol | | 1.9E−04 |
| | +1 × 6 nm polymeric sol | | |
| E6a–E6d | 1 × 85 nm nano-dispersion | 1400 °C | 1.4E−05 |
| | +1 × 65 nm nano-dispersion | | 1.6E−05 |
| | +1 × 35 nm colloidal sol | | 7.8E−06 |
| | +1 × 6 nm polymeric sol | | 1.3E−05 |
| E7a | 2 × 65 nm nano-dispersion | 1300 °C | 6.5E−04 |
| | +2 × 35 nm colloidal sol | | |
| | +2 × 6 nm polymeric sol | | |
| E8a | 1 × 85 nm nano-dispersion | 1300 °C | 4.9E−04 |
| | +1 × 65 nm nano-dispersion | | |
| | +1 × 35 nm colloidal sol | | |
| | +1 × 6 nm polymeric sol | | |
| Conventional | 1 × 260 nm suspension | 1400 °C | 1E−05–1E−06 |
| 7–10 μm thick electrolyte made by vacuum slip casting [26] | | | |
| Conventional | 1 × 260 nm paste | 1400 °C | 1E−05–1E−07 |
| 7–10 μm thick electrolyte made by screen printing [26] | | | |

layer was ∼2 μm and thus also significantly larger as in the previous examples E4 and E5.

Samples with a polymeric sol coating were also tested after firing at 1200 °C and 1300 °C. After firing at 1200 °C, all samples were He untight, which could be due to the presence of scattered a number of untight areas, which increase dramatically the He leakage. The first 1300 °C samples showed a He leakage of $4.9 \times 10^{-4}$ and $6.5 \times 10^{-4}$ (hPa dm$^3$)/(s cm$^2$), which confirms the potential of the described coating processes, when a reduction of the firing temperature is desired.

## 4. Discussion

Based on previous observations, it is clear that significant progress has been achieved in the development of thin film 8YSZ electrolyte layers for SOFCs. This achievement is mainly based on the selection of an additive, which gives in combination with the prepared nano-dispersions and sols a perfect coating behaviour in the dip-coating and spin-coating step, irrespective of the rough and very porous surface of the anode. The efficiency of the developed coating process was evident from SEM analysis of the calcined layers, which indicated that unwanted infiltration of the nanoparticles into the pores of the AFL could be avoided and very homogeneous precursor layers were formed.

During the development stage of the coating process, it was actually attempted to find an alternative for methods, which involve the modification of a very porous substrate with a polymeric filler material or a wax. At the end, a very practical method was obtained, which provides a potential to scale up and which shows also some additional advantages. First, a common water soluble polymeric compound is used, which can be simply burned out at 500 °C, without disturbing the layer. We also experienced that a rapid thermal heating program can be

used for this purpose. Second, problems with wetting behaviour of a substrate with temporarily filled pores are avoided. Third, problems with adhesion of the layer after the coating process on a modified substrate are avoided.

In comparison with conventional powder coating methods, the developed nanoparticle process shows also significant advantages. First, the ability to deposit much smaller nanoparticles makes it possible to form thinner porous precursor layers, which give of course thinner dense layers after sintering. For example, in experiments with 85 nm and 60 nm nano-dispersions, fully sintered 8YSZ layers with an average thickness of ~2 μm and ~1 μm were obtained, while the thickness of comparable conventional layers is typically in the range 10–30 μm, depending on the literature source.

Another important aspect is that the nanoparticle process gives much finer porous precursor layers compared with a conventional coating method. In a typical powder coating method, with a particle size of several 100 nm, a pore size >100 nm is obtained, while the precursor layer made from the 60 nm nano-dispersion has e.g. a pore size of 6–7 nm. The impact thereof on the sintering behaviour was also clearly observed. Despite the lack of He tight layers, SEM pictures of several layers fired at 1200 °C, particularly those made with the 60 nm nano-dispersion and with sols, showed almost dense layers with sub-micrometer grains at 1200 °C. After firing at 1300 °C, 8YSZ grains grew to the micrometer range, which resulted in the formation of mainly dense 8YSZ electrolyte layers with a thickness of just one single grain. A reduction of the firing temperature to this range would for example also allow the use of a steel-supported anode.

Despite these improvements, a sintering temperature of 1300–1400 °C seems to be very high, since 1400 °C is typically applied in a conventional SOFC preparation route. It can be assumed however that several mechanisms operate concurrently during sintering. When we consider transport by diffusion as the main mechanism for densification, it is clear that small particles provide small diffusion paths and therefore enhance the sintering (e.g. [20,22]). On the other hand, a requirement is that the particles are densely packed to minimize the pore volume – while maximizing the number of particle contact points – and we observed a fast coarsening of the layer at 1200 °C, characterized by grain growth and pore growth, which of course competes with densification.

The role of the substrate was not directly investigated in this study, but was also evident from the obtained results. First, the roughness of the substrate appears to play a role, since a number of untight areas have been observed in areas where the substrate shows a strong curvature. On the other hand, the shrinkage of the substrate seems also to be a major factor. The effect of substrate shrinkage on the formation of thicker dense 8YSZ layers is well-known and has also been previously described for the same warm-pressed substrate[23,24] and in the literature for similar substrates.[25] At 1200 °C and 1300 °C, shrinkage of the substrate is limited and most samples in our work were also not completely densified. At 1400 °C, on the other hand, no untight areas were observed and the layers showed a good He tightness, while a considerable shrinkage of the substrate is obtained as previously described in the mentioned references. Continuing work on the deposition and sintering of nanoparticle 8YSZ layers on non-shrinking substrates, e.g. steel-supported anode layers, is in this regard highly interesting.

## 5. Conclusion

A practical and scalable wet coating process has been developed, for the deposition of gas-tight thin film 8YSZ electrolyte layers on regular anode substrates. Such layers have a thickness of 1–2 μm and sinter to full density at 1400 °C, which is also the typical firing temperature in a conventional SOFC preparation route. Furthermore, enhanced densification in the temperature region 1200–1300 °C was found, which can be attributed to the reduced particle and pore size of the precursor 8YSZ layer, in comparison with conventional powder coating processes. Based on the obtained coating experience, an approach was adopted which includes the deposition of a first 8YSZ layer starting from an 85 nm or 60 nm nano-dispersion and then to coat additionally 8YSZ sol–gel layers. Co-firing at 1200 °C lead to fully sintered layers with sub-micrometer grains, based on SEM observations. Further examination of the layers with He leakage tests indicated however that a number of untight areas are still present on a macroscopic scale. After firing at 1300 °C, the 8YSZ grains grow to the micrometer range, which resulted in the formation of dense 8YSZ electrolyte layers with a thickness of just one single grain.

## Acknowledgements

Robert Mücke and Sebastian Vieweger are acknowledged for their assistance with profilometry measurements and He leak testing. Stefan Roitsch (Ernst Ruska-Centre) is thanked for making the TEM pictures. The colleagues from the SOFC group are thanked for providing the substrates.

## References

1. Wachsman ED, Singhal SC. Solid oxide fuel cell commercialization, research and challenges. *Am Ceram Soc Bull* 2010;**89**(3):22–32.
2. Yamamoto O. Solid oxide fuel cells: fundamentals and prospects. *Electrochim Acta* 2000;**45**:2423–35.
3. Steele BCH, Heinzel A. Materials for fuel-cell technologies. *Nature* 2001;**414**:345–52.
4. Menzler NH, Tietz F, Uhlenbruck S, Buchkremer HP, Stöver D. Materials and manufacturing technologies for solid oxide fuel cells. *J Mater Sci* 2010;**45**:3109–35.
5. Tietz F, Fu Q, Haanappel VAC, Mai A, Menzler NH, Uhlenbruck S. Materials development for advanced planar solid oxide fuel cells. *Int J Appl Ceram Technol* 2007;**4**(5):436–45.
6. Kueper TW, Visco SJ, De Jonghe LC. Thin-film ceramic electrolytes deposited on porous and non-porous substrates by sol–gel techniques. *Solid State Ionics* 1992;**52**:251–9.
7. De Jonghe LC, Jacobson CP, Visco SJ. Supported electrolyte thin film synthesis of solid oxide fuel cells. *Annu Rev Mater Res* 2003;**33**:169–82.
8. Peters C, Weber A, Butz B, Gerthsen D, Ivers-Tiffée E. Grain-size effects in YSZ thin-film electrolytes. *J Am Ceram Soc* 2009;**92**(9):2017–24.
9. Noh H-S, Son J-W, Lee H, Song H-S, Lee H-W, Lee J-H. Low temperature performance improvement of SOFC with thin film electrolyte

and electrodes fabricated by pulsed laser deposition. *J Electrochem Soc* 2009;**156**(12):B1484–90.
10. Heiroth S, Lippert T, Wokaun A, Döbeli M. Microstructure and electrical conductivity of YSZ thin films prepared by pulsed laser deposition. *Appl Phys A* 2008;**93**:639–43.
11. Ignatiev A, Chen X, Wu N, Lu Z, Smith L. Nanostructured thin solid oxide fuel cells with high power density. *Dalton Trans* 2008:5501–6.
12. Gannon P, Sofie S, Deibert M, Smith R, Gorokhovsky V. Thin film YSZ coatings on functionally graded freeze cast NiO/YSZ SOFC anode supports. *J Appl Electrochem* 2009;**39**:497–502.
13. Park Y-i, Chen Su P, Cha SW, Saito Y, Prinz FB. Thin-film SOFCs using gastight YSZ thin films on nanoporous substrates. *J Electrochem Soc* 2006;**153**:A431–6.
14. Su P-C, Chao C-C, Shim JH, Fasching R, Prinz FB. Solid oxide fuel cell with corrugated thin film electrolyte. *Nano Lett* 2008;**8**(8):2289–92.
15. Chun S-Y, Mizutani N. The transport mechanism of YSZ thin films prepared by MOCVD. *Appl Surf Sci* 2001;**171**:82–8.
16. Schafbauer W, Menzler NH, Buchkremer HP. Influence of thermal treatment during cell manufacturing on the performance of tape cast solid oxide fuel cells. *ECS Trans* 2009;**25**(2):649–54.
17. Van Gestel T, Sebold D, Meulenberg WA, Buchkremer H-P. Development of thin-film nanostructured electrolyte layers for application in anode-supported solid oxide fuel cells. *Solid State Ionics* 2008;**179**: 428–37.
18. Van Gestel T, Han F, Sebold D, Buchkremer HP, Stöver D. Nano-structured solid oxide fuel cell design with superior power output at high and intermediate operation temperatures. *Microsyst Technol* 2011;**17**(2):233–42.
19. Van Gestel T, Sebold D, Kruidhof H, Bouwmeester HJM. $ZrO_2$ and $TiO_2$ membranes for nanofiltration and pervaporation: Part 2. Development of $ZrO_2$ and $TiO_2$ toplayers for pervaporation. *J Membr Sci* 2008;**318**:413–21.
20. Brinker CJ, Scherer GW. Sol–gel science: the physics and chemistry of sol–gel processing. San Diego: Academic Press; 1990.
21. Van Gestel T, Sebold D, Hauler F, Meulenberg WA, Buchkremer H-P. Potentialities of microporous membranes for $H_2/CO_2$-separation in future fossil fuel power plants: evaluation of $SiO_2$, $ZrO_2$, $Y_2O_3$–$ZrO_2$ and $TiO_2$–$ZrO_2$ sol–gel membranes. *J Membr Sci* 2010;**359**:64–79.
22. Boutz MMR, Olde Scholtenhuis RJM, Winnubst AJA, Burggraaf AJ. A hydrothermal route for production of dense, nanostructured Y-TZP. *Mater Res Bull* 1994;**29**:31–40.
23. Mücke R, Menzler N, Buchkremer HP, Stöver D. Cofiring of thin zirconia films during SOFC manufacturing. *J Am Ceram Soc* 2009;**92**:95–102.
24. Mücke R, Menzler N, Buchkremer HP, Stöver D. Sintering of thin zirconia SOFC electrolyte films. *ECS Trans* 2007;**7**(1):2175–85.
25. Tikkanen H, Suciu C, Waernhus I, Hoffmann AC. Examination of the co-sintering process of thin 8YSZ films obtained by dip-coating on in-house produced NiO-8YSZ. *J Eur Ceram Soc* 2011;**31**:1733–9.
26. Mücke R. Sintering of zirconiumoxide electrolytes in the multilayer structure of SOFCs. PhD Dissertation, Ruhr-University Bochum; 2007.